Journal of Membrane Science 326 (2009) 58–63

Contents lists available at ScienceDirect

Journal of Membrane Science

journal homepage: www.elsevier.com/locate/memsci

High-performance silicon nanopore hemofiltration membranes

William H. Fissell[a,b,*], Anna Dubnisheva[b], Abigail N. Eldridge[b], Aaron J. Fleischman[b], Andrew L. Zydney[c], Shuvo Roy[b,d]

[a] Department of Nephrology and Hypertension, Cleveland Clinic, Cleveland, OH 44195, United States
[b] Department of Biomedical Engineering, Cleveland Clinic, Cleveland, OH, United States
[c] Department of Chemical Engineering, Pennsylvania State University, University Park, PA, United States
[d] Department of Bioengineering & Therapeutic Sciences, University of California, San Francisco, CA, United States

ARTICLE INFO

Article history:
Received 7 May 2008
Received in revised form 5 September 2008
Accepted 12 September 2008
Available online 30 September 2008

Keywords:
Hemofiltration
Artificial kidney
Nanotechnology
MEMS
Silicon

ABSTRACT

Silicon micromachining provides the precise control of nanoscale features that can be fundamentally enabling for miniaturized, implantable medical devices. Concerns have been raised regarding blood biocompatibility of silicon-based materials and their application to hemodialysis and hemofiltration. A high-performance ultrathin hemofiltration membrane with monodisperse slit-shaped pores was fabricated using a sacrificial oxide technique and then surface-modified with poly(ethylene glycol) (PEG). Fluid and macromolecular transport matched model predictions well. Protein adsorption, fouling, and thrombosis were significantly inhibited by the PEG. The membrane retained hydraulic permeability and molecular selectivity during a 90-h hemofiltration experiment with anticoagulated bovine whole blood. This is the first report of successful prolonged hemofiltration with a silicon nanopore membrane. The results demonstrate feasibility of renal replacement devices based on these membranes and materials.

1. Introduction

The kidney is unique in that it is the first organ for which long-term *ex vivo* substitutive therapy has been available and lifesaving. Significant progress has been made to slow or prevent progression to end-stage renal disease (ESRD), yet in 2004, 335,963 patients in the United States were dependent on maintenance dialysis for life [1]. Renal transplantation confers excellent survival, but is severely limited by scarcity of donor organs. The great majority of patients with chronic renal failure require dialysis. Patient outcomes in dialysis have been disappointing, with an annual mortality exceeding 25% [2].

Several studies have shown improved clinical outcomes when hemodialysis is delivered for several hours every day ("quotidian dialysis") compared to the conventional, thrice-weekly therapy. Pierratos and colleagues demonstrated improved nutrition, bone mineral metabolism, blood pressure control, and regression of left ventricular hypertrophy with high dose therapy, and retrospective comparisons suggest greatly improved survival when compared with conventional thrice-weekly dialysis [3–7].

Widespread use of prolonged or continuous therapies will likely require significant miniaturization of the renal replacement technology so that devices can ultimately be used in a wearable or implantable format. This requires significant improvements in membrane properties to achieve the ultrafiltrate flux, solute transport rates, and immunoisolation required in this application. Conventional polymer filtration membranes have polydisperse and irregularly shaped pores, making it difficult to achieve the desired hydraulic permeability while maintaining an absolute barrier to macromolecular passage. Track-etched membranes can largely eliminate polydispersity in pore size, but the membranes tend to be fairly thick (approximately 10 μm) and they must have low porosity (<2%) to minimize the formation of overlapping pores (ion tracks) that would compromise membrane selectivity and immunoisolation [9].

Silicon bulk and surface micromachining and microfabrication techniques, collectively referred to as the microelectromechanical systems (MEMS) toolkit, provide unprecedented control over nanoscale feature size and geometry in a scalable manufacturing process. The control of pore geometry can potentially provide novel opportunities to optimize molecular transport rates. A membrane with uniform pores can reduce resistance to fluid flow while maintaining molecular selectivity compared to polydisperse porous materials. Controlled pore shape, such as elongated or slit-shaped pores, also provide additional reductions in hydraulic resistance when compared with round or irregular pores. Thus,

* Corresponding author at: Department of Nephrology and Hypertension, Cleveland Clinic, Cleveland, OH 44195, United States. Tel.: +1 216 445 2206; fax: +1 216 444 9198.
E-mail address: fisselw@ccf.org (W.H. Fissell).

0376-7388/$ – see front matter © 2008 Elsevier B.V. All rights reserved.
doi:10.1016/j.memsci.2008.09.039

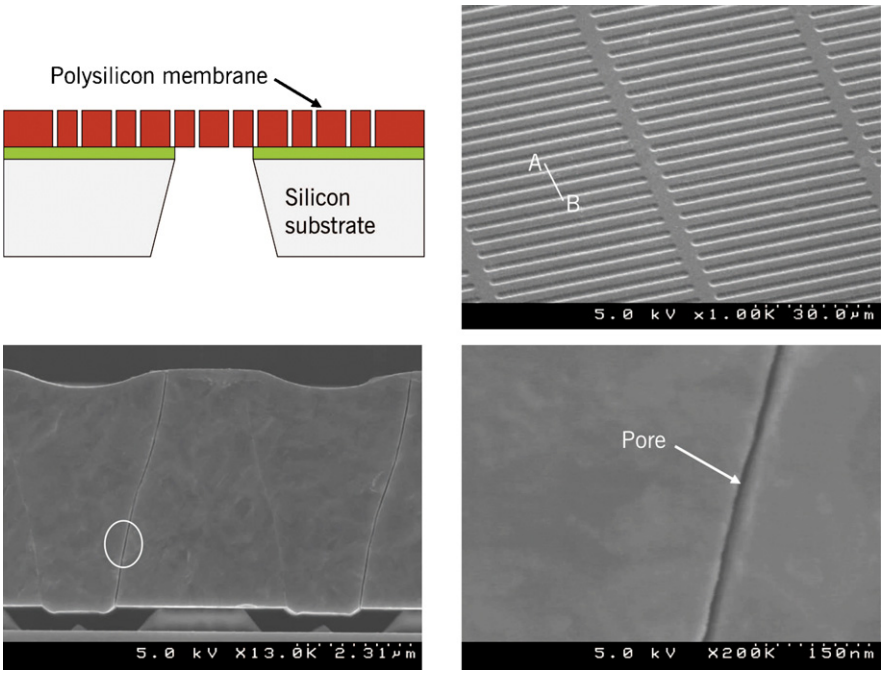

Fig. 1. Nanopore membrane fabricated using silicon MEMS technology. *Top left*: Cross-section of membrane illustrating various structural layers (not to scale). Pores (exaggerated) are formed in the polysilicon diaphragm, which is supported by an underlying silicon substrate. *Top right*: SEM image of membrane showing uniformly spaced array of slit pores. *Bottom left*: SEM image showing membrane cross-section and non-tortuous pore geometry. *Bottom right*: SEM image showing close-up of 9 nm slit pore and smooth surface characteristics.

MEMS-based membranes are fundamentally enabling for miniaturization of renal replacement devices to a wearable or implantable size, whether for conventional therapies or for an implantable artificial kidney. The biocompatibility of silicon-based MEMS substrates has been previously assessed using international standards, with the results suggesting that these materials are inert and relatively nontoxic [10].

In this study, we examine the performance of nanoporous membranes with long, slit-shaped pores that offer significant theoretical advantages over round pores in terms of hydraulic permeability and molecular selectivity [11,12]. Data are also presented for the effects of a covalent poly(ethylene glycol) surface modification on the overall blood compatibility of these novel membrane materials and their ability to retain selectivity and hydraulic flow during prolonged (90-h) hemofiltration experiments with anticoagulated blood. Membranes were tested for a duration of 90 h, which is comparable to the lifetime of commercial dialyzer membranes, to determine if permselectivity and hydraulic permeability were stable over that period of time.

2. Materials and methods

2.1. Fabrication of nanopore membranes and thin film substrates

Silicon nanopore membranes (SNMs) have been prototyped from silicon substrates by an innovative process based on MEMS technology as previously reported (Fig. 1) [13–16]. The process uses the growth of a thin sacrificial SiO_2 (oxide) layer to define the critical nanoscale pore size of the filter. The oxide is etched away in the final step of the fabrication process to leave behind open slit pores. Thermal oxidation of silicon substrates can routinely provide oxides down to 5-nm thickness with <1% variation across a 100-mm diameter wafer.

Standard microfabrication processes to prepare thin film samples have previously been described in detail [15]. Such samples were used to study albumin binding and contact activation of the coagulation cascade as reported herein. Briefly, a lot of virgin, prime grade, single side polished, 100-mm diameter, 500-μm thick, ⟨1 0 0⟩-oriented, n-type, silicon (Si) wafers was cleaned using a conventional "piranha" clean procedure, which involved a 20-min immersion in 3:1 H_2SO_4/H_2O_2 mixture, followed by thorough rinse in deionized (DI) water and drying with nitrogen gas. Afterwards, the wafers were further cleaned using a dual stage "RCA" clean procedure, which removed any residual surface organic and inorganic contaminants. Thermal oxidation was then conducted to grow SiO_2 films on some wafers, while polysilicon films were deposited on other wafers using a low pressure chemical vapor deposition (LPCVD) process. An additional wafer received no further processing. The wafers were subsequently cut into 1 cm × 1 cm chips. Subsets of these 1 cm^2 ⟨1 0 0⟩ Si, SiO_2, and polysilicon chips were either set aside unmodified ("bare") or poly(ethylene glycol) (PEG)-modified as described below. This chipset represents all the material types in the nanomembrane that contact blood.

2.2. Surface modification

To limit membrane fouling by globular proteins, the surfaces of materials in the chipset described above were covalently modified with PEG using a previously reported solution phase method, modified to omit all sonication steps and continuing the PEG deposition for 12 h [17]. A number of previous studies have demonstrated that attachment of PEG can significantly reduce protein adsorption and improve biocompatibility of a variety of surfaces [18–21]. The technique used for PEG attachment involved a single-step mechanism which covalently couples silicon surface silanol groups (Si–OH) to a PEG polymer through a trimethoxysilane group forming a Si–O–Si–PEG sequence by a methanol dehydration reaction.

2.3. Protein sieving and hemofiltration

Membrane arrays were examined under differential interference contrast light microscopy for defects. Membrane hydraulic

permeability was evaluated using phosphate buffered saline (PBS), with the flow rate evaluated by timed collection over a range of pressures from 3.4 to 13.8 kPa. The data were used to calculate the mean pore size, h, as

$$h = \left(\frac{12\mu L}{w}\frac{\Delta Q}{\Delta P}\right)^{1/3} \quad (1)$$

where L (membrane thickness) and w (long dimension of the slit pore) were measured by scanning electron microscopy, μ is the viscosity of the PBS, and $\Delta Q/\Delta P$ is the slope determined by linear regression of the observed flow rate versus pressure data [22,23].

Solute transport measurements were obtained using membranes mounted in an ultrafiltration cell. The retentate side of the membrane was continuously perfused at a flow rate of 1 ml/min from a 100 ml reservoir containing 50 μg/ml polydisperse fluorescein isothiocyanate (FITC)-labelled Ficoll 70 in bovine whole blood anticoagulated with ACD-A citrate. The permeate side of the membrane was wetted with a measured volume of PBS. Citrate was chosen as an anticoagulant since its effects can be easily reversed by addition of calcium to the anticoagulated blood, facilitating comparison of this data with results in future experiments. Compressed dry air was used to generate a transmembrane pressure of 13.8 kPa (2 psi) as monitored by a pressure transducer (Entran, EPX 10PG, Les Clayes-sous-Bois, France) within the filtration cell. The ultrafiltration volume was monitored in a calibrated syringe barrel (Hamilton, Reno, NV, USA) capped with parafilm. Additional tests with feed solutions of 500 μg/ml each of carbonic anhydrase ("CA", MW = 29 kD; No. C3934, Sigma), bovine serum albumin ("BSA", MW = 66 kD, No. A5378, Sigma), and thyroglobulin ("TG", MW = 670 kD, No. T1001, Sigma) in PBS were completed to compare observed molecular transport with published transport models. Feed and permeate samples were analyzed by gel permeation chromatography with an Ultrahydrogel 500 column using a 600E controller and 474 fluorescence detector (Waters Corp., Milford, MA). Size calibration of the column for Ficoll was performed with monodisperse Ficolls of known sizes, which were the kind gift of Dr. Bengt Rippe, Lund University, Lund, Sweden.

Membranes were removed from the filtration cell after testing, rinsed with deionized water, dried, and examined for adherent cells and thrombus by scanning electron microscopy (SEM). Protein adsorption to the blood and protein filtration membranes was assessed by scanning electron microscopy and X-ray photoelectron spectroscopy (XPS).

2.4. Protein adsorption

Protein adsorption to the materials tested was measured following the technique of Sharma et al. [21]. Samples of 1 cm × 1 cm bare and PEG-modified chips were rinsed with DI water and air-dried. The bare (unmodified) polysilicon and SiO_2 samples were piranha cleaned as above and rinsed 3× with DI water and air-dried. Both sets of substrates were then placed in 12-well plates with 1.0 ml of 0.5 mg/ml FITC-labeled bovine serum albumin ('FITC-BSA", Sigma Aldrich) in PBS (pH 7.4). These samples were then incubated at 37 °C in 5% CO_2/95% air for 1 h, as previous studies have suggested that BSA adsorption to similar substrates reaches steady state in significantly less than one hour [24]. After removal from the incubator each chip was rinsed three times in PBS and placed in a new 12-well plate with 1 ml of PBS. This entire process was done with minimal light in order to limit photobleaching of the FITC-BSA. Tissue culture polystyrene (TCPS) forms a convenient positive control as it is widely available and has been treated in the manufacturing process to avidly adsorb proteins. TCPS (Cat #3513, Corning Inc Life Sciences, Acton, MA) was incubated with FITC-BSA as described above and used as a positive control to normalize collected data.

Imaging was conducted within 20 min of removal from the incubator. Each chip was mounted on a glass microscope slide with one drop of PBS and a glass cover slip. Images were collected using a Leica DMR Upright Microscope (Leica-Microsystems, Heidelberg, GmbH) with a Retiga EX cooled CCD camera (QImaging, Burnaby, BC, Canada) and an HC PL Fluotar 20× 0.5 NA dry objective. Five images for each sample were obtained for each of $n = 3$ samples of bare polysilicon, PEG-modified polysilicon, and tissue culture polystyrene.

ImagePro Plus software (Media Cybernetics, Silver Spring, MD) was used to analyze the average pixel intensities of 12-bit images from each substrate. Pixel intensities were averaged to quantify protein binding for each substrate type. All controls and experimental chips were imaged on the same day using identical parameters and exposure times. Albumin binding to bare and PEG-modified substrates was expressed as percentage of albumin binding to tissue culture polystyrene.

In order to measure biofouling of the membranes, XPS was used to asses the surface chemistry of fresh membranes and membranes after 100 h of hemofiltration using anticoagulated blood. X-ray photoelectron spectra were obtained with a PHI-5600 XPS (Physical Electronics, Inc., Chanhassen, MN) system. A take off angle of 45° was used with a monochromatic Al Kα X-ray (1486.6 eV) with an emission current of 17.0 μA and an electron energy of 8.0 eV to minimize charging. Survey spectra were collected from 0 to 1100 eV with a pass energy of 93.9 eV.

2.5. Blood coagulation

Contact activation of the coagulation cascade by bare and PEG-modified ⟨1 0 0⟩-oriented Si samples, as well as glass cover slips, was measured by plasma recalcification time as described by Xu et al. [25], but measured by appearance of a visible clot of fibrin versus an initial strand. Briefly, blood samples were obtained from a healthy donor into citrated tubes and promptly centrifuged at 3000 rpm at 8 °C for 20 min to obtain platelet-poor plasma (PPP). 100 μL of warmed (37 °C) PPP and 25 μL of warmed 100 mM $CaCl_2$ in water were pipetted onto the substrate surface and incubated at 37 °C for 10 min. The plasma droplet was monitored for clot formation by dipping a 27-gauge needle that had been formed into a hook into the droplet and observing for a fibrin clot on the hook.

2.6. Statistics

Experiments were repeated in triplicate and protein assays in duplicate. Means, standard deviations, and statistical tests were calculated using Microsoft Excel 2003 for Windows.

3. Results and analysis

3.1. Fabrication of nanopore membranes

Membrane characteristics and hydraulic permeability analysis have been previously reported [13–16]. After fabrication, the silicon wafer is sized into 1 cm × 1 cm chips bearing arrays of 1 mm × 1 mm nanopore membranes. Each membrane is a ~4-μm thick polysilicon diaphragm, which incorporates an array of ~10 nm × 45 μm slit pores uniformly spaced with ~2 μm separation (Fig. 1). The pores exhibit smooth surfaces and minimal tortuosity through the thickness of the membrane. Pore size distribution in the membrane is dependent on the thickness variation in sacrificial oxide, which showed less than 1% mean variation (Fig. 2). Actual pore size of individual membranes were verified by hydraulic permeability analysis, and subsequently confirmed by SEM imaging of the chips. Membranes tested for this paper had measured hydraulic

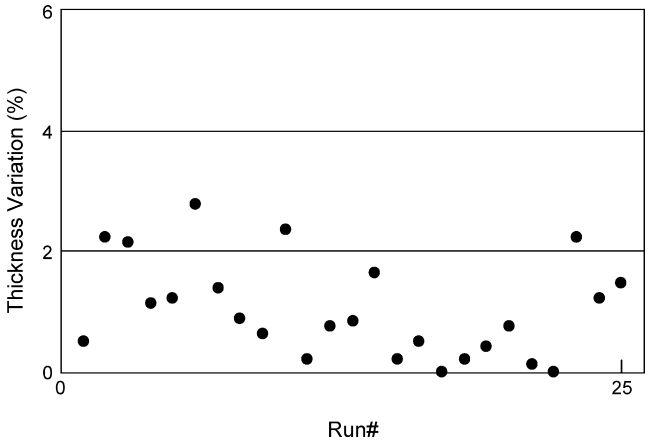

Fig. 2. Pore size distribution in nanopore membranes. Graph showing minimal variation in thickness of sacrificial oxide, which establishes the monodisperse pore size. The oxide film exhibits a <1% mean variation (3% maximum) in thickness across 100-mm diameter wafers over 25 separate runs in an thermal oxidation furnace.

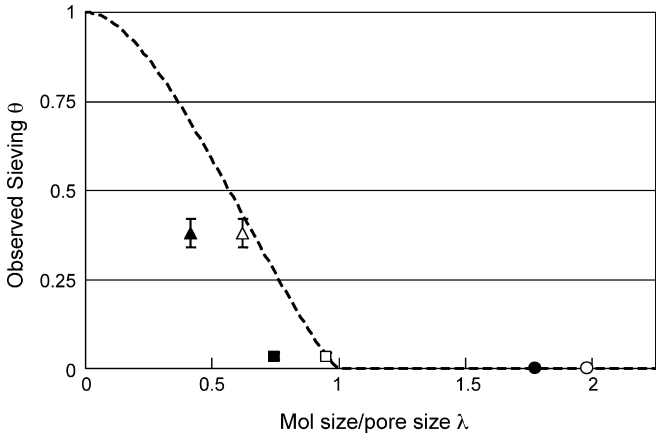

Fig. 3. Protein sieving by 9.7-nm silicon nanopore membrane. Observed sieving coefficient, θ, is plotted versus the ratio of Stokes diameter to pore size, λ, for a 9.7-nm PEG-modified nanopore membrane. Three globular proteins, carbonic anhydrase (MW = 29 kD, triangles), bovine serum albumin (MW = 66 kD, squares) and thyroglobulin (MW = 669 kD, circles) were rejected by the membrane in a size-dependent manner (solid symbols, means ± standard errors). When the molecular size is modeled as the Stokes–Einstein diameter of the protein plus the thickness of the electrical double layer (open symbols, means ± standard errors), the results are in good agreement with model predictions.

permeabilities closely matching estimates of pore size from process control variables and SEM imaging.

3.2. Solute transport

Solute transport was evaluated at a 13.8 kPa driving pressure, giving a filtrate flux of approximately $J_v = 1.0 \times 10^{-7}$ m/s. Spatial average velocity inside the pore is estimated to be approximately two orders of magnitude higher, reflecting the membrane's low porosity. Shear rates in the feed compartment were estimated to be 0.5 s^{-1} at the 1 ml/min feed flow rate. This corresponds to a mass transfer coefficient of approximately $k_m = 5.2 \times 10^{-7}$ m/s as evaluated from the Leveque solution for fully developed channel flow [12]:

$$k_m = 0.807\left(\frac{D^2\gamma_w}{L}\right)^{1/3} \quad (2)$$

where D is the protein diffusion coefficient, γ_w is the wall shear rate in the feed channel, and L is the channel length. Thus, a reasonable estimate of concentration polarization effects is $C_w/C_b \approx 1.2$ for a fully retained solute with $D \approx 10^{-10}$ m^2/s where C_w is the solute concentration immediately adjacent to the membrane and C_b is the solute concentration in the bulk (feed) solution. Under the testing conditions, the membrane Peclet number Pe_m, for bovine albumin is approximately 10^1, suggesting that convective transport dominates and our observed sieving coefficients reflect the intrinsic membrane rejection characteristics [12]. The observed sieving coefficient will be approximately equal to the product of the solution partition coefficient (Φ) and the hindrance factor for convection (K_c) since concentration polarization and transmembrane diffusion were both negligible in this experimental system. Dechadilok and Deen published analytic expressions for ΦK_c, as well as diffusive hindrances, for a variety of solute/pore geometries, including results for a rigid sphere in a slit-shaped pore which accurately describes our experimental system [26]:

$$\Phi K_c = 1 - 3.02\lambda^2 + 5.776\lambda^3 - 12.3675\lambda^4 + 18.9775\lambda^5 - 15.2185\lambda^6 + 4.8525\lambda^7 + O[\lambda^8] \quad (3)$$

where λ is the ratio of molecule diameter to the critical pore dimension, analogous to $\lambda = r_s/r_p$ for cylindrical pores.

PEG-modified membranes displayed size-dependent rejection of globular proteins. Model predictions overestimated the sieving coefficients for the globular proteins (carbonic anhydrase, bovine serum albumin, and thyroglobulin) through the silicon nanopore membrane (filled symbols in Fig. 3). We hypothesize that this behavior is due to electrostatic interactions associated with the distortion of the diffuse electrical double layer around the charged proteins [27,28]. A simple approximate analysis of these electrostatic interactions, in which the protein size is increased by the thickness of the electrical double layer (EDL) around the protein, gives model predictions that match the experimental observations closely (open symbols in Fig. 3) [14,26].

Membranes retained their size-dependent rejection of Ficoll during prolonged (90 h) pressure-driven filtration of bovine whole blood (Fig. 4). Ficoll retention was greater after blood contact and the sieving profile was sharper, compared with prior observations in PBS alone, an effect previously reported by Langsdorf et

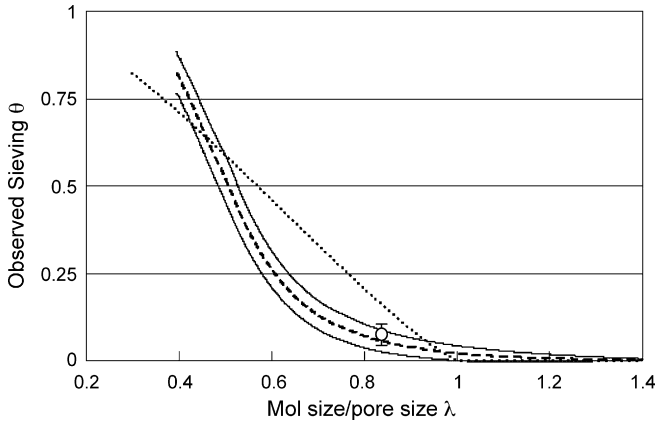

Fig. 4. Hemofiltration of Ficoll and albumin by 10.9-nm silicon nanopore membrane. Observed sieving coefficient, θ, is plotted versus the ratio of Stokes diameter to pore size, λ, for a 10.9-nm PEG-modified nanopore membrane. FITC-Ficoll 70 was added to citrated bovine whole blood and the mixture filtered by a PEG-modified 10.9-nm pore size membrane. Size-dependent rejection of Ficoll 70 was observed, but displayed reduced transmission of Ficoll (solid lines, mean ± standard deviation) and albumin (open circle, mean ± standard deviation) when compared with filtration in PBS (this figure and Fig. 3). The dashed curve represents model predictions for convective solute transport.

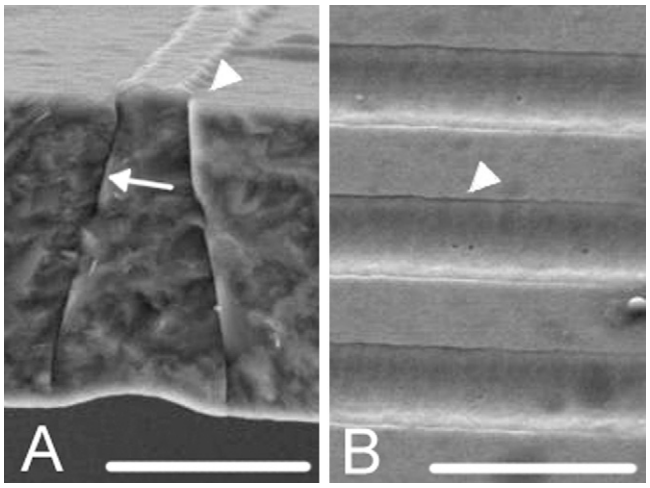

Fig. 5. Silicon nanopore membrane after blood filtration. Scanning electron micrographs of blood (A) and filtrate (B) sides of a 10.9 nm pore size membrane after >100 h of continuous blood filtration. A highly uniform thin film appears to coat the blood-side surface of the membrane (A, arrowhead), but does not appear to extend into the pores (A, arrows), scale bar = 3 μM. The filtrate side appears free of adherent proteins, and the pores are easily visualized (B, arrowhead), scale bar = 5 μM.

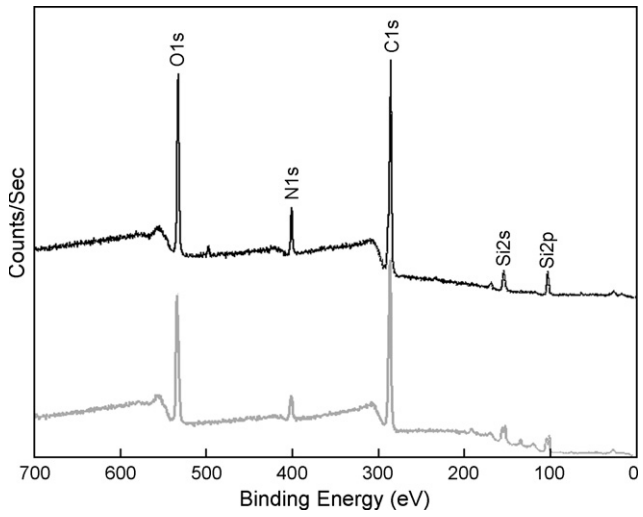

Fig. 6. X-ray photoelectron spectroscopy of silicon nanopore membrane before and after blood filtration. X-ray photoelectron spectra of PEG-modified membranes were obtained after (black line) >100 h of blood filtration and compared with spectra of membranes exposed to PBS only (light grey line). Spectra were similar in oxygen, carbon, and nitrogen content, but the N 1s peak was slightly higher (6.7% vs. 5.9%) in the blood-exposed samples, suggesting that the thin film observed in Fig. 5 was at least partially composed of protein.

al. for both cellulose and AN69 hemodialysis membranes [14,29]. For example, the ratio of the sieving coefficient of a 100 kDa Ficoll to that of a 25 kDa Ficoll was 0.05 when measured using bovine blood compared to a value of only 0.40 when measured using PBS. This increased selectivity may be related to changes in the membrane transport properties associated with the formation of a protein deposit on and within the membrane pores, as discussed by Langsdorf et al. [14,29], which is clearly seen in the SEM images in Fig. 5.

Alternatively, the reduction in filtrate flux for the experiments performed with blood would reduce the extent of concentration polarization and Ficoll elongation. The observed sieving coefficient for albumin with bovine blood was 0.07 ± 0.03, which closely matches the Ficoll results when the albumin size is calculated as the Stokes–Einstein diameter plus the thickness of the surrounding electrical double layer. Hydraulic permeability of the membrane was unchanged during 90 h of continuous blood filtration (first run flux = 9.99×10^{-6} m/s compared to the last run flux = 9.99×10^{-6} m/s). These results demonstrate that the presence of the PEG significantly limits membrane fouling even upon prolonged exposure to blood.

3.3. Protein adsorption

FITC-BSA adsorption to a positive control, tissue culture polystyrene, was demonstrated by uniform bright fluorescence. PEG-modification of silicon substrates was confirmed by X-ray photoelectron spectroscopy (PHI-5600, Physical Electronics, Chanhassen, MN) (data not shown). PEG modification reduced FITC-BSA binding on SiO_2 substrates from $24.9 \pm 12.5\%$ of positive control (untreated silica) to $4.4 \pm 1.2\%$ (PEG-modified silica) ($p < 10^{-6}$, Student's *t*-test), and from $10.6 \pm 0.2\%$ of positive control (untreated polysilicon films) to $4.4 \pm 1.5\%$ (PEG-modified polysilicon films) ($p < 10^{-5}$, Student's *t*-test).

3.4. Blood coagulation

Plasma recalcification time of bare ⟨1 0 0⟩ silicon substrates was similar to that measured for glass cover slips (720 ± 17 s vs. 610 ± 26 s), but was significantly prolonged (>3600 s) for PEG-modified ⟨1 0 0⟩ silicon ($p < 10^{-6}$, by Student's *t*-test). After an hour, no visible clot had formed on the PEG-modified samples, but the recalcified plasma droplets had begun to evaporate, and the experiment was terminated. Scanning electron microscopy of membranes after blood filtration revealed a thin film adherent to the blood side of the membranes (Fig. 5). The permeate side of the membrane and the interior of the membrane pores appeared unchanged. X-ray photoelectron spectra of PEG-modified membranes exposed to blood and to PBS alone were similar in oxygen, carbon, and nitrogen content (Fig. 6), but the N 1s peak was slightly higher (6.7% vs. 5.9%) in the blood-exposed samples, suggesting that the thin film observed in Fig. 5 was at least partially composed of protein.

4. Discussion

A novel fabrication toolkit, MEMS, was used to fabricate filtration membranes with unprecedented control of pore size and geometry. A simple, easily executed surface modification protocol involving the attachment of polyethylene glycol nearly eliminated protein fouling and contact activation by the silicon membranes. These membranes were successfully used for prolonged (up to 90 h) hemofiltration using anticoagulated blood, providing the first demonstration that these silicon nanoporous membranes might be suitable for use in long-term or implantable applications.

Although the membranes used in these studies are not appropriate for immediate use in an implantable artificial kidney, the results from this study suggest that it should be possible to develop silicon-based membranes with the desired physical and transport characteristics using MEMS technology. First, the albumin sieving data confirm that existing models for steric interactions, such as those by Deen [22,23,26], allow prediction of the maximum pore size that will reject albumin, guiding engineering of the albumin-retentive membrane needed for this application. The required pore size will be a function of the ionic strength of the solution, the surface charge of the final membrane material, and blood–membrane

interactions during filtration. Accordingly, the optimum pore size is likely only slightly smaller than the 9.7–10.9 nm pore sizes of the membranes examined in this paper and well within the capabilities of the MEMS toolkit.

Second, the close agreement between hydraulic permeability theory and experiment allows estimation of package size for an implanted filter using capillary perfusion pressure as the driving force for ultrafiltration. Using Poiseuille's law, we can calculate the number of pores needed to achieve clinically relevant ultrafiltration rates, say 30 ml/min at 30 mm Hg driving pressure, at about 5×10^{10} pores. With typical modern nanoscale fabrication, feature sizes enabled by state-of-the-art MEMS, and nanofabrication technology should be able to provide $\sim 10^{11}$ pores (7 nm $\times$ 40 μm) in a 0.1-m^2 membrane, which is a reasonable size for implantation. Thus, the data reported here demonstrate that the end goal of our research is feasible. That is, it should be possible to develop a hemofiltration membrane delivering useful filtration rates under cardiovascular driving pressures in a package size suitable for implantation using the silicon MEMS toolkit.

Third, the applicability of silicon as the substrate material for hemofiltration and dialysis membranes has been questioned previously, since the SiO_2 that forms naturally as a thin layer on exposed silicon surfaces is a potent activator of the coagulation cascade. While the data presented here are far from conclusive, it appears that the silicon surface can be modified, in this case using polyethylene glycol, to dramatically attenuate contact activation and fouling. The initial success with this technique lends support to continued development of renal replacement membranes using the silicon MEMS toolkit.

Future studies will be needed to examine the issues of concentration polarization in more detail, including the changes in flow rates and mass transfer characteristics caused by the cellular components in blood. Careful design of the flow path may be needed to minimize polarization effects at high filtrate flux. There are also important questions about the long-term mechanical stability of the membranes, particularly when fabricated with very large pore densities and reduced thickness.

Competing interests statement

The following authors: WHF, AJF, and SR are inventors on one or more patents related to the subject material in this paper, and are entitled to a share of any royalty payments that may derive from commercialization of the patent(s). The results presented in this paper have not been published previously in whole or part, except in abstract format.

Acknowledgements

This work was supported by grants: 1K08 EB003468 (National Institute of Biomedical Imaging and Bioengineering, NIH), 1 R01 EB008049-01 (National Institute of Biomedical Imaging and Bioengineering, NIH), and W81XWH-05-2-0010 (U.S. Army Medical Research and Materiel Command, DoD).

References

[1] C.Y. Hsu, et al., The incidence of end-stage renal disease is increasing faster than the prevalence of chronic renal insufficiency, Annals of Internal Medicine 141 (2) (2004) 95–101 (see comment).
[2] U.S. Renal Data System, USRDS 2007 Annual Data Report: Atlas of End-Stage Renal Disease in the United States, National Institutes of Health, National Institute of Diabetes and Digestive and Kidney Diseases, Bethesda, 2007.
[3] C.T. Chan, et al., Regression of left ventricular hypertrophy after conversion to nocturnal hemodialysis, Kidney International 61 (6) (2002) 2235–2239.
[4] A.P. Heidenheim, et al., Patient quality of life on quotidian hemodialysis, American Journal of Kidney Diseases 42 (1 Suppl.) (2003) 36–41.
[5] R.M. Lindsay, et al., Calcium and phosphate balance with quotidian hemodialysis, American Journal of Kidney Diseases 42 (1 Suppl.) (2003) 24–29.
[6] A. Pierratos, et al., Quotidian dialysis—update 2005, Current Opinion in Nephrology & Hypertension 14 (2) (2005) 119–124.
[7] D. Somers, On the nature of the glomerular barrier to albuminuria: electrokinetic glomerulus theory, Journal of the American Society of Nephrology 16 (2005) 109a.
[9] J. Han, et al., Molecular sieving using nanofilters: past, present and future, Lab on a Chip 8 (1) (2008) 23–33.
[10] G. Kotzar, et al., Evaluation of MEMS materials of construction for implantable medical devices, Biomaterials 23 (13) (2002) 2737–2750.
[11] W.H. Fissell, et al., Development of continuous implantable renal replacement: past and future, Translational Research: The Journal of Laboratory & Clinical Medicine 150 (6) (2007) 327–336.
[12] L.J. Zeman, A.L. Zydney, Microfiltration and Ultrafiltration, Marcel Dekker, New York, 1996.
[13] W. Fissell, et al., Initial characterization of a nanoengineered ultrafiltration membrane, Journal of the American Society of Nephrology 13 (2002) 602A.
[14] W.H. Fissell, et al., Ficoll is not a rigid sphere, American Journal of Physiology. Renal Physiology 293 (4) (2007) F1209–F1213.
[15] W.H. Fissell, et al., Differentiated growth of human renal tubule cells on thin-film and nanostructured materials, ASAIO Journal 52 (3) (2006) 221–227.
[16] J.M. Magistrelli, Investigating fluid flow through silicon nanoporous membranes, in: Chemical Engineering, Case Western Reserve University, Cleveland, OH, 2004.
[17] A. Papra, N. Gadegaard, N.B. Larsen, Characterization of ultrathin poly(ethylene glycol) monolayers on silicon substrates, Langmuir 17 (2001) 1457–1460.
[18] K.C. Popat, et al., Poly(ethylene glycol) interfaces: an approach for enhanced performance of microfluidic systems., Biosensors & Bioelectronics 19 (9) (2004) 1037–1044.
[19] S. Sharma, et al., Nanostructured antifouling poly(ethylene glycol) films for silicon-based microsystems, Journal of Nanoscience & Nanotechnology 5 (2) (2005) 235–243.
[20] S. Sharma, et al., XPS and AFM analysis of antifouling PEG interfaces for microfabricated silicon biosensors, Biosensors & Bioelectronics 20 (2) (2004) 227–239.
[21] S. Sharma, et al., Evaluation of the stability of nonfouling ultrathin poly(ethylene glycol) films for silicon-based microdevices, Langmuir 20 (2) (2004) 348–356.
[22] M. Davidson, W. Deen, Hindered diffusion of water-soluble macromolecules in membranes, Macromolecules 21 (1988) 3474–3481.
[23] W. Deen, Hindered transport of large molecules in liquid-filled pores, AIChE Journal 33 (1987) 1409–1425.
[24] R. Kurrat, J. Prenosil, J. Ramsden, Kinetics of human and bovine serum albumin adsorption at silica–titania surfaces, Journal of Colloid and Interface Science 185 (1996) 1–8.
[25] F.J. Xu, et al., Heparin-coupled poly(poly(ethylene glycol) monomethacrylate)–Si(1 1 1) hybrids and their blood compatible surfaces, Biomacromolecules 6 (3) (2005) 1759–1768.
[26] P. Dechadilok, W. Deen, Hindrance factors for diffusion and convection in pores, Industrial Engineering and Chemical Research 45 (2006) 6953–6959.
[27] D. Burns, A. Zydney, Contributions to electrostatic interactions on protein transport in membrane systems, AIChE Journal 47 (2001) 1101–1114.
[28] N.S. Pujar, A.L. Zydney, Electrostatic effects on protein partitioning in size-exclusion chromatography and membrane ultrafiltration, Journal of Chromatography A 796 (2) (1998) 229–238.
[29] L.J. Langsdorf, L.G. Krankel, A.L. Zydney, Effect of blood–membrane interactions on solute clearance during hemodialysis, ASAIO Journal 39 (3) (1993) M767–M772.